JOURNAL OF Applied Polymer SCIENCE

Investigation of Mechanical Properties of Alumina Nanoparticle-Loaded Hybrid Glass/Carbon-Fiber-Reinforced Epoxy Composites

Akash Mohanty,[1] Vijay Kumar Srivastava,[1] Pulya Umamaheswara Sastry[2]
[1]Department of Mechanical Engineering, Indian Institute of Technology (BHU), Varanasi 221005, India
[2]Solid State Physics Division, Bhabha Atomic Research Centre, Trombay, Mumbai 400085, India
Correspondence to: A. Mohanty E-mail: (amohanty.rs.mec@iitbhu.ac.in).

ABSTRACT: This research work investigates the tensile strength and elastic modulus of the alumina nanoparticles, glass fiber, and carbon fiber reinforced epoxy composites. The first type composites were made by adding 1–5 wt % (in the interval of 1%) of alumina to the epoxy matrix, whereas the second and third categories of composites were made by adding 1–5 wt % short glass, carbon fibers to the matrix. A fourth type of composite has also been synthesized by incorporating both alumina particles (2 wt %) and fibers to the epoxy. Results showed that the longitudinal modulus has significantly improved because of the filler additions. Both tensile strength and modulus are further better for hybrid composites consisting both alumina particles and glass fibers or carbon fibers. © 2013 Wiley Periodicals, Inc. J. Appl. Polym. Sci. **2014**, *131*, 39749.

KEYWORDS: composites; fibers; mechanical properties

Received 16 March 2013; accepted 9 July 2013
DOI: 10.1002/app.39749

INTRODUCTION

Epoxy-based hybrid composites are extensively used in many engineering and industrial applications in recent times. Excellent adhesive compatibility between the matrix materials and the reinforcing elements as well as better mechanical strength are the key factors that make these composites the best choice for load bearing complex engineering applications. However, the existing virgin materials are not capable enough to cater to the new challenges like providing high quality tailor-made mechanical strength at the point of interest. Hence, there is growing demand to design and fabricate high quality reliable materials. Short-fiber-reinforced polymers have found their way into lightly loaded secondary structures in which stiffness dominates the design, but notable increase in strength as compared to the un-reinforced polymer is required. It has been reported that the incorporation of fillers like metal particles, fibers, and nanomaterial-coated fibers results in the formation of composites with better mechanical properties.[1,2] Various studies involving optimization of the volume/weight fraction of the reinforcing elements within the polymeric matrix have also been reported.[3] For example, Zhou et al.[4] proposed that mere 2 wt % of carbon nanofiber filler can improve the tensile and fatigue strengths of epoxy composite by 11% and 22% respectively. The other advantages of these materials are low cost, flexibility to incorporate as a variety of reinforcing elements, and easy fabrication.[5,6] Similarly, alumina (Al_2O_3) nanoparticles are widely used engineering ceramic filler materials because of their ability to make the composite with high elastic modulus, high wear resistance, chemical corrosion resistance,[7] stability, and retention of strength at high temperatures. However, higher brittleness and accumulation of particles during the fabrication process cause limitations in its usage.[8] In order to understand the stress transfer behavior and improvement in the mechanical properties, many experimental and theoretical studies were done on fiber and particle-loaded composite materials.[9–12] Recently, the short-fiber-reinforced thermoplastics are being used extensively as they not only offer superior mechanical properties but also can be produced easily by rapid, low-cost extrusion compounding, and open moulding process. Thus, this has motivated many researchers to investigate the role of combining nanoparticles and short fibers as fillers on the mechanical strength of the composites.[4,8,13–16]

In this article, we have investigated the influence of alumina particles, short glass fiber and carbon fiber fillers on the tensile strength of epoxy matrix. For this purpose, different types of the composite plates were fabricated by varying the volume fraction of the filler contents. The microstructure of the alumina-loaded composites has been characterized by small-angle X-ray scattering and other complementary techniques.

EXPERIMENTAL

Materials

For the fabrication of the composite, the epoxy matrix, which is a blend of unmodified solvent free epoxy resin with specific gravity 1.14 (trade name of Bondtite PL-411)[17] and the amine-based hardener with specific gravity 0.98 (grade PH-861)[18] procured from Resinova Chemie, India, has been used. The composition of the base matrix formulation was the mixture of 10–12 parts by weight of the hardener with the epoxy, which provides the pot life of 30 min at room temperature. For the alumina-based composites, as received alumina particles of size 25–90 μm with the surface area 265 m^2/g, supplied by Sasol-Germany, was used. These micron-sized alumina particles were reduced to nanometer size during processing of the composite plates. For Fiber composites, commercially available electrical grade glass fiber and PAN-based carbon fibers supplied by Zoltek-USA, were used as the reinforcing elements. The mechanical properties and the density of the components used to fabricate the composites have been reported in literature.[15,19,20]

Fabrication of Composites Plates

Initially, the reinforcing elements and fillers were dried in a furnace for 4 h at 80°C. The resin was preheated up to 50°C for 20 min to achieve a lower viscosity and the better wetability properties. The glass fibers and carbon fibers of size 1–7 mm underwent degassing in the vacuum oven. Alumina powder of 1%, 2%, 3%, 4%, and 5% by wt. was added to the epoxy matrix during the continuous mechanical stirring operation. Consequently, PH-861 hardener was added to the mixture, followed by the continuous mechanical stirring and degassing. Short glass and carbon fibers were incorporated into the matrix by the similar way. In the hybrid composite, fiber content was varied from 1 wt % to 5 wt % keeping alumina powder fixed at 2 wt %. The mixture was poured into the firmly clamped dual piece symmetrical metallic mould containing a rectangular pocket of required dimension, lubricated with silicon oil. Care was taken to nullify the chance of entrapped air particles during the pouring process and the cast moulds were kept at room temperature for 24 h for the preliminary curing purposes.

Preparation and Postcuring Operation of Test Specimens

In order to prepare the test specimens from the flat composite sheets using the water-lubricated profile cutter, the ASTM D 638 standard has been followed. The postcuring operation of the composite plates has been carried out by keeping them inside the vacuum furnace, followed by the slow cooling in a controlled atmosphere.[19,20] The sets of five identical test specimens were prepared from the identical composite panels.

Estimation of Void Content

The void fraction in the composites has been calculated by using ASTM D2734-09 standard[21] from the formula:

$$V = 100(T_d - M_d)/T_d \quad (1)$$

where V is the percentage by volume of void content, T_d is the theoretical density (g/cm^3), and M_d is the measured density (g/cm^3). While preparing the test coupons for the measurement of tensile strength, composite plates possessing void content less than 5% by volume were selected.

Small Angle X-ray Scattering

Small angle X-ray (SAXS) measurements were carried out using a goniometer mounted on Rigaku rotating anode X-ray generator (CuKα). Composites consisting 1–5 wt % of alumina were used for the measurements. Scattered X-ray intensity I (q) was recorded using a scintillation counter with pulse height analyzer by varying the scattering angle 2θ, where q is the scattering vector equal to $4\pi.\sin(\theta)/\lambda$ and λ is the wavelength of incident X-rays. The intensities were corrected for sample absorption and smearing effects of collimating slits.[22]

Fourier Transform Infrared Spectra

In order to find the changes in the molecular structure because of alumina content, Fourier transform infrared (FTIR) spectra were recorded using the Thermo Scientific Nicolet 6700 FT-IR spectrometer.

Transmission Electron Microscope

Transmission electron microscope (TEM) pictures were recorded using a machine of type FEI Tecnai™ TEM G2 series operated at 200 kV, equipped with liquid nitrogen cooled sample holder.

Tensile Test

The tensile strength and Young's modulus of the composites were measured using the twin lead screw table top UTM of make Zwick/Roell Z010 with 10-kN load cell capacity with a crosshead speed of 1.3 mm/min. The average value for five test specimens of identical composition was recorded for the analysis.[23–25]

RESULTS AND DISCUSSION

Figure 1 shows a typical TEM image of the composite with alumina particles, which shows that the size of the filler particles is

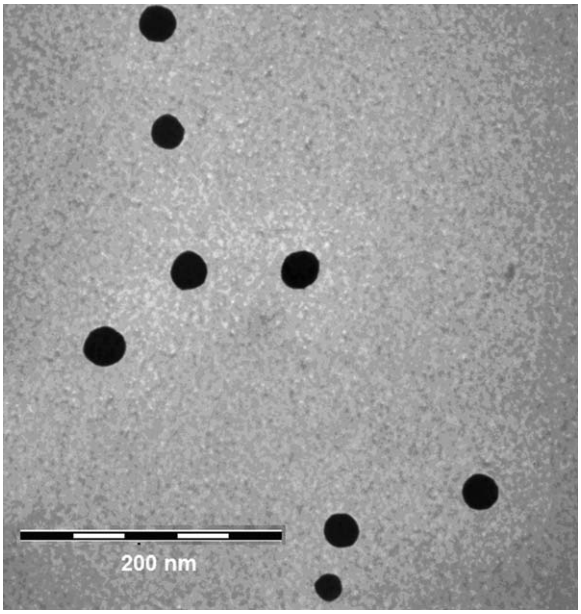

Figure 1. TEM image the epoxy composite containing 2 wt % alumina nanoparticles.

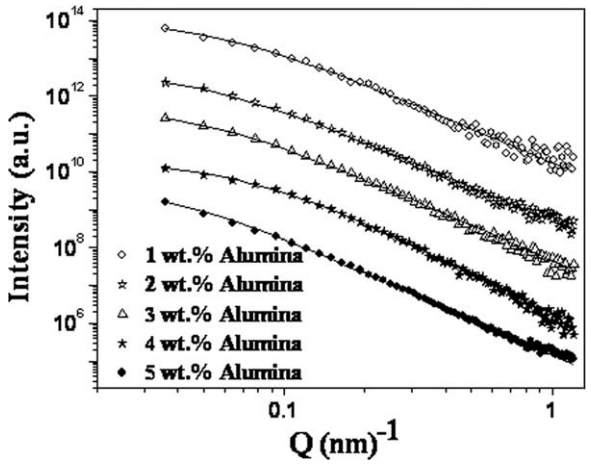

Figure 2. Small angle x-ray scattering of alumina (%) in epoxy matrix. (Symbols are experimental points and lines are fits.)

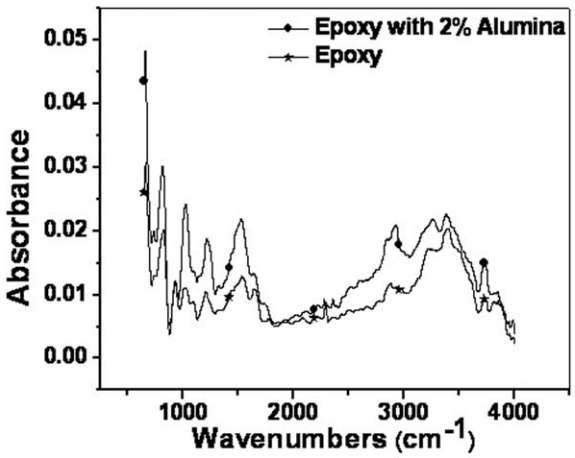

Figure 3. FTIR spectra of pure epoxy and nano-alumina-epoxy composite.

in the range of 20–40 nm. Further details of the structure were obtained from the analysis of SAXS data. For obtaining the structural characteristics of aluminium particles, the data of the composites were subtracted from that of pure matrix. Figure 2 shows the SAXS profiles displayed on a log–log scale. For scattering from particles with smooth surface, the intensity $I(Q)$ in the high-Q region follows a power-law, $I\ (Q) \sim Q^{-\alpha}$ with α equals to 4. However, for the present composites, α is found to be noninteger varying between 3 and 4 suggesting the surface fractal nature with rough surfaces of the particles.[23–26] The fractal dimension Ds, which is a measure of the surface roughness, is given as $Ds = (6 - \alpha)$. Thus, the value of Ds is 2 for smooth surfaces and 3 for maximum roughness. In order to obtain the average size of the particles, the SAXS profiles of all the samples are fitted to the modified Debye function [eq.(2)].[26–29]

$$I(q)=I(0)/\left[1+(\xi q)^2\right]^{-a/2} \quad (2)$$

The particle radius (R) can be found from the relation [eq.(3)].

$$\xi^2=[(1+\alpha)/3]\times R^2 \quad (3)$$

Figure2 shows the fitted data and the parameters obtained are listed in Table I. It may be noticed that the size of the particles vary between 25 and 32 nm for the samples having alumina content up to 4%, whereas with 5% alumina, the particle size has increased to 46 nm. The order of magnitude of the particle sizes is in concurrence with TEM results. The increased particle size for composites with 5 wt. % of alumina is because of the aggregation of individual particles.

Table I. Parameters Obtained from SAXS

Alumina (wt %)	2.R (nm)	Ds
1	25	2.7
2	32.5	2.9
3	32.5	2.9
4	25	2.66
5	46	2.88

Figure 3 shows typical FTIR spectra of epoxy resin and epoxy with 2 wt % of alumina nanoparticles. The peaks are identified with –OH stretching band around 3500 cm^{-1}, the C–H band stretching of SP_2 around 3055 cm^{-1} and the C–H band stretching of SP_3 around 2950, 2873 cm^{-1}, respectively.[30] The peak because of the aromatic C=C band stretching can be seen between 1608 and 1456 cm^{-1}, because of the C–O band stretching at around 1290 cm^{-1}, whereas the peak around 900 cm^{-1} corresponds to the presence of epoxide groups in the epoxy resin.

After the addition of alumina nanoparticles, the intensities of the peaks at 900, 1290 cm^{-1} and in the aromatic region i.e. 1608–1456 cm^{-1} considerably increase and additional weak peaks corresponding to the band stretching of –CN bonds at around 2237 cm^{-1} and that of C=O bonds at around 1723 cm^{-1} are noticed. This suggests a possible interaction between the alumina nanoparticles and the epoxy matrix.

Properties of the Composites

Influence of the Fillers on the Density of the Composites. The variation of the density of the composites with the volume fractions of the fillers is shown in Figure 4. It may be noticed that the density increases linearly with increase in the concentration of the fillers. For instance, after loading 4% volume fraction of alumina particles, carbon fiber and glass fiber, and the density of the epoxy matrix increases to 11%, 5.8%, and 2.6%, respectively.[26] This increase in the density, which originates from the matrix curing process, is expected to make a significant impact on the over-all performance of the composites.

Influence of the Volume Shrinkage on the Failure Strain of the Composite. The effect of the shrinkage volume on the failure strain of the composites is shown in Figure 5. The shrinkage volume is a phenomenon which is observed during the curing process of the composite.[31] The reaction of the hardener with neat epoxy results in the modification of the chemical structure and evolution of gases. As the chemical reaction is neutralized, the net volume decreases. From Figure5, it may be noticed that the variation in the failure strain is least for carbon-fiber-

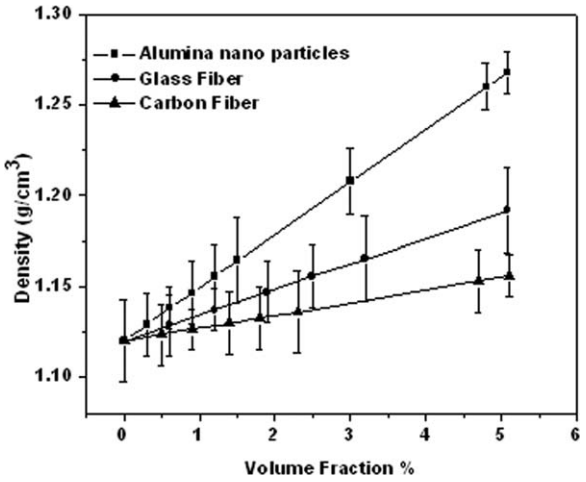

Figure 4. Variation of density with volume fraction of fillers.

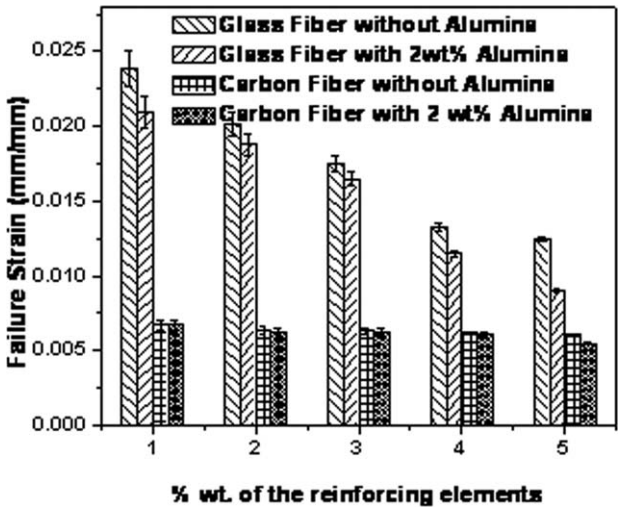

Figure 6. Effect of the % wt. of fillers on the failure strain of various composites.

reinforced composites. With the incorporation of the 2 wt % of alumina along with the carbon fibers, no significant improvement in properties has been noticed. However, the glass-fiber-reinforced composites showed substantial improvements on the bulk properties.

Effect of Filler Addition on the Failure Strain of the Composite. Figure 6 shows the effect of the filler addition on the failure strain of the composites. It is observed that the failure strain decreases gradually with the addition of the fibers to the neat epoxy. It is also interesting to observe that the reduction of the failure strain is more in case of glass fiber-epoxy composite. A further reduction is observed because of the addition of 2 wt % alumina nanoparticles to glass fiber and epoxy mixture, whereas the improvement is marginal after the addition of alumina particles to carbon-fiber-reinforced composites.

Calculation of Fiber Efficiency *P*arameter. Normally, the reinforcement efficiency of the fiber-based composites is difficult to calculate. However, it is usually represented by a parameter known as fiber efficiency parameter (K) that depends on V_f and the E_f/E_m ratio. From these parameters, the elastic modulus of the composites is given by

$$E_{\text{Composite}} = K \times \left(E_m \times V_m + E_f \times V_f\right) \tag{4}$$

where V_f, V_m, E_f, and E_m are the volume fraction of fiber, volume fraction of matrix, elastic modulus of the fiber, and elastic modulus matrix, respectively.

The volume fractions of the fillers were calculated from the weight fraction by considering the density of the individual constituents of the composite. From Figure 7, it may be noticed that with the increase in the volume fraction, that the value of K varies marginally for the alumina-loaded composites where as it decreases in a nonlinear way for the carbon fiber composites. For glass fiber composite, K increases initially up to 2% volume fraction and then remains constant with further loadings. These results suggest that the alumina nanoparticles dispersed more uniformly than glass fiber and carbon fiber in the matrix.

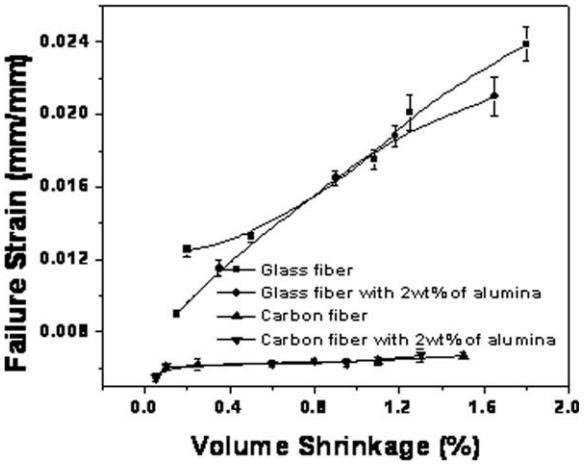

Figure 5. Effect of the % volume shrinkage on the failure strain of various composite systems: (a) pure glass fiber; (b) glass fiber with 2 wt % of alumina; (c) pure carbon fiber; and (d) carbon fiber with 2 wt % of alumina.

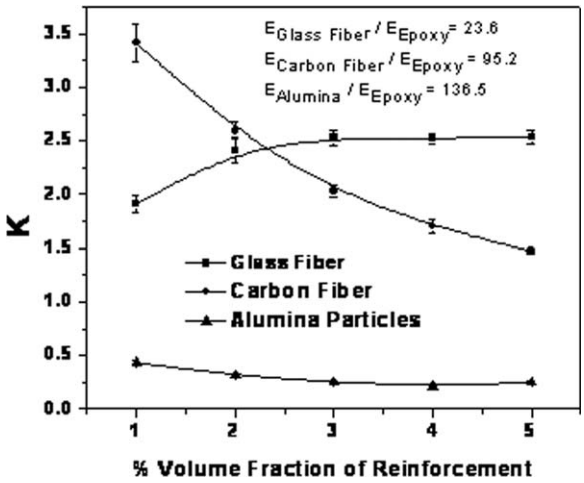

Figure 7. Effect of the volume fraction of the reinforcing elements on the fiber efficiency parameter K.

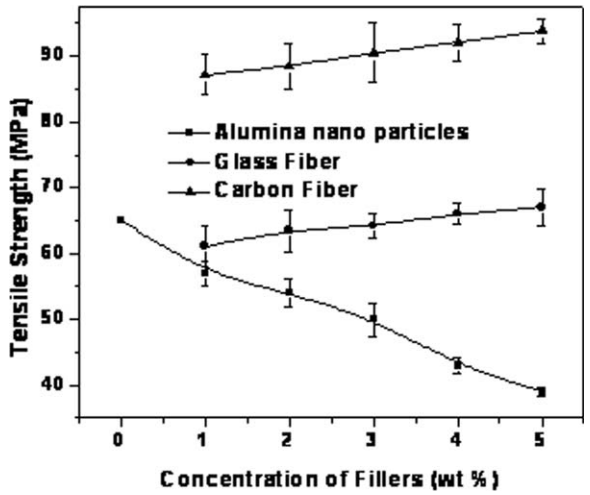

Figure 8. Tensile strength of various composite systems.

Effect of Nano*p*articles and Fibers on the Tensile Strength. Figure 8 shows the change in the tensile strength with the concentration of the fillers. It is observed that the tensile strength gradually decreases with the addition of alumina and increases with the inclusion of fibers. The decrease in the strength may be because of the agglomeration with the addition of more and more nanoparticles, which provides higher surface area available for the entrapment of macro-sized air bubbles from the atmosphere. This causes a reduction in the net strength of the composite. It is noteworthy that agglomeration of alumina particles above 4 wt % addition of the filler has also been supported by SAXS. In the case of fiber composites, the fibers act as the load carrier and improve the tensile modulus.

Effect of Filler Addition on the Tensile Strength and Modulus of the Composite. Figure 9(a) shows the effect of addition of 2 wt % alumina nanofillers on the tensile strength of the fiber composites. It is noticed that addition of alumina has no

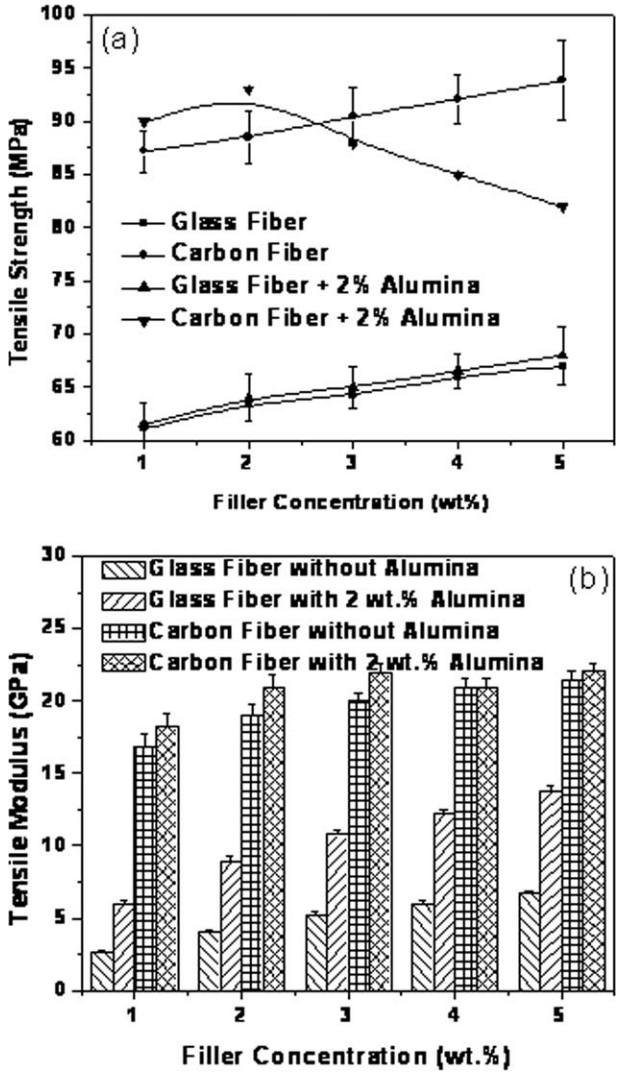

Figure 9. Effect of filler concentration on the (a) tensile strength and (b) longitudinal modulus of various composite systems.

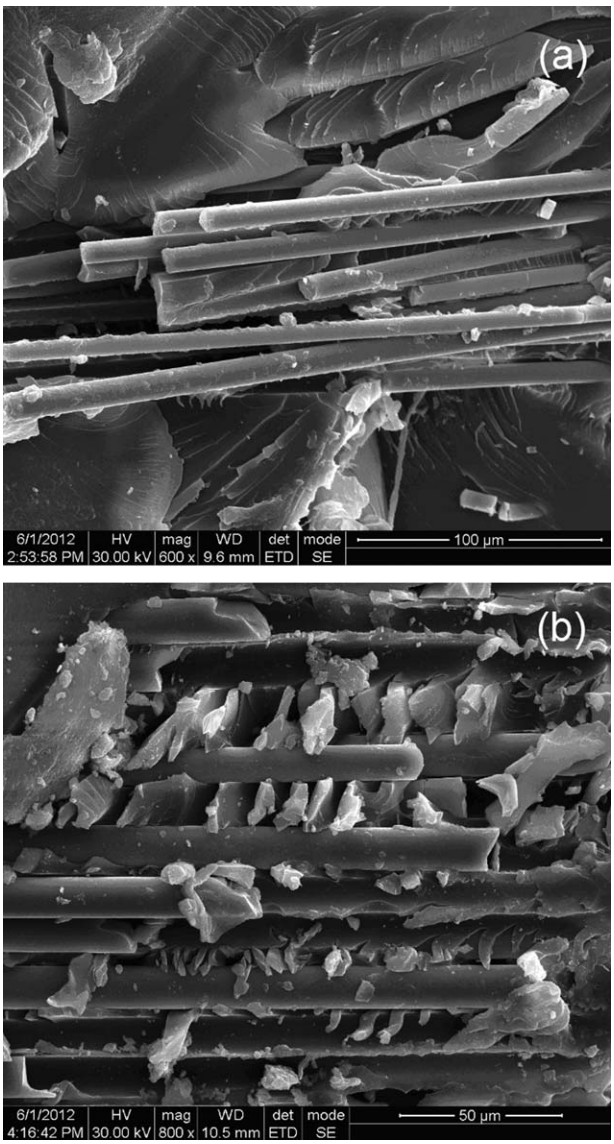

Figure 10. SEM image of the fractured test specimen because of (a) fiber failure and (b) matrix cracking.

significant impact on the the strength of glass fiber composites. For carbon fiber composites, the strength marginally increases up to 2 wt % of the fiber and it decreases rapidly at higher concentrations. This drop in the strength may be because of the agglomeration of nanoparticles and the proximity to the formation of fiber bundles. The other reason for the reduction of strength may be because of hindrance caused for the easy escape of the volatile gases evolved during the curing process at higher loadings of the reinforcing elements. However the failure of the nanoparticles and fiber-reinforced hybrid composites might be because of the combined mode of the fiber and matrix failure thus absorbs more energy to cause complete failure of the composites.

Figure 9(b) shows the tensile modulus of the composites at various filler concentrations. It is noticed that the tensile modulus improves with the incorporation of fillers in all the cases and the gain is further enhanced in hybrid type of composite. Figure 10 shows typical SEM images of the fractured test specimens.

Based on the above findings, a schematic representation of the combined effect of the inter-phase layers of nanoparticles and fiber-reinforced composites is depicted in Figure 11. We propose that, the improvement in the tensile properties with 2 wt % addition of alumina nanoparticles in the fiber composites may be because of the availability of the larger specific surface area of the nanofillers and optimum dispersion of filler/reinforcing elements in the matrix as confirmed by SAXS and TEM analysis. Under the stressed condition, the propagation of the crack may occur in two ways; by the de-bonding (phase separation) of the nanoparticles and matrix or propagation through either individual particles or agglomerated clusters [Figure 11(a)]. However the de-bonding of the constituents of the composites under stressed condition unlikely to occur because of the perfect bonding of nanoparticles in the epoxy matrix. Figure 11(b) depicts the mechanism of the energy absorption corresponding to the 2 wt % of alumina filler along with the fibers. Thus, under the condition of uniformly distributed nanoparticles, the bifurcation of rapidly growing cracks absorbs more energy to cause the delayed mechanical failure of the composite. This mechanism offers larger fracture surface area during the crack propagation and consumes a greater amount of energy, mainly because of the congested plastic deformation of matrix materials.[32,33]

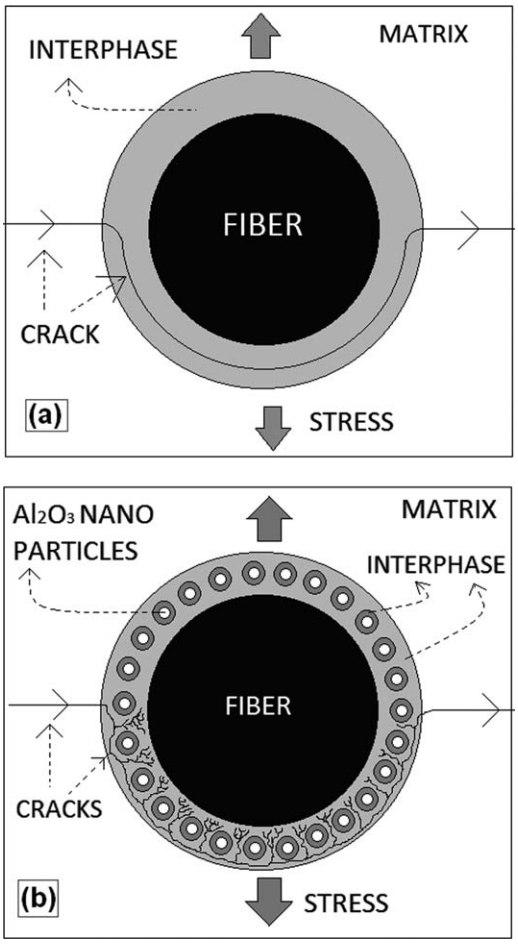

Figure 11. Schematic illustration of energy dissipation and stress transfer in the interphase layer of fiber composites (a) without and (b) with nanoparticle-reinforced epoxy composite.

CONCLUSIONS

The tensile strength and modulus of alumina particles, fiber-loaded epoxy composites have been investigated in detailed. The optimum mechanical properties are achieved by systematically varying the volume fraction of the fillers in the epoxy matrix. The major findings are summarized below:

1 Small angle X-ray scattering of alumina-reinforced epoxy composites shows the presence of particles of size 25–50 nm with rough surfaces. The particle size increases with the increase in the wt % of alumina particles.
2 The strain at failure and the volume shrinkage increases gradually with the increase of the filler contents but it remains constant for hybrid type of composites.
3 Addition of alumina nanoparticles to the epoxy matrix has a significant effect on the improvements of mechanical properties. The tensile strength and modulus of glass fiber, carbon-fiber-loaded composites were further increased because of the addition of 2 wt % alumina particles.
4 Fiber efficiency parameter K of the composites has been estimated and its variation with concentration of the fillers has been studied. The variation of K is found to be more significant with fiber fillers than with alumina particles in the matrix.

An extensive study on the performance of this type of hybrid composite under adverse condition may be an interesting topic of the future research.

ACKNOWLEDGMENTS

One of the authors, Mr. Akash Mohanty would like to acknowledge the department of mechanical engineering, IIT (BHU), Varanasi, India, for the raw materials and technical support, Mr. A. K. Patra from SSPD, B.A.R.C., India, for his help in carrying out the SAXS experiments, SAIF IIT Madras (established by DST, India) for providing the SEM facility.

REFERENCES

1. Rahaman, A.; Kar, K. *Fulle. Nano Carbon Nanostruct.* **2011**, *19*, 373.
2. Lubineau, G.; Rahaman, A. *Carbon* **2012**, *50*, 2377.
3. Friedrich, K; Zhang, Z; Schlarb, A. K. *Compos. Sci. Technol.* **2005**, *65*, 2329.
4. Zhou, Y.; Pervin, F.; Jeelani, S.; Mallick, P. K. *J. Mater. Proc. Technol.* **2008**, *198*, 445.
5. Fereshteh-Saniee, F.; Majzoobi, G.H.; Bahrami, M. *J. Mater. Proc. Technol.* **2005**, 162–163, 39–45.
6. Fu, S. Y.; Lauke B. *Compos. Part A.* **1998**, *29A*, 575.
7. C'urković L; Kumic' I; Grilec K. *Ceram. Int.* **2011**, *37*, 29.
8. Zhao, S.; Zhang, J.; Zhao, S.; Li, W.; Li. H. *Compos. Sci. Technol.* **2003**, *63*, 1009.
9. Ogasawara, T.; Ishida, Y.; Kasai, T. *Compos. Sci. Technol.* **2009**, *69*, 2002.
10. Li, X. F.; Lau, T. K.; Yin, Y. S. *Compos. Sci. Technol.* **2008**, *68*, 2876.
11. Zhao, S.; Schadler, L. S.; Duncan, R.; Hillborg, H.; Auletta, T. *Compos. Sci. Technol.* **2008**, *68*, 2965.
12. Cortés, D. A.; Hogg, P. J.; Tanner, K, E.; Ren, G. *Mater. Des.* **2007**, *28*, 1547.
13. Fu, S. Y.; Yue, C.; Hu, X. *J. Mater. Sci. Let.* **2001**, *20*, 31.
14. Fu, S. Y.; Lauke, B. *Composites* **1998**, *29A*, 575.
15. Cho, J.; Joshi, M. S.; Sun, C. T. *Comp. Sci. Technol.* **2006**, *66*, 1941.
16. Asi, O. *J. Reinf. Plast. Comp.* **2009**, *28*, 2861.
17. Hernanz, R. P.; Serna, J. G.; Dodds, Christopher; Hyde, J.; Poliakoff, M.; Cocero, M. J.; Kingman, S.; Pickering, S.; Lester, E. *J. Supercrit. Fluids* **2008**, *46*, 83.
18. Garcia, F. G.; Silva, P. M.; Soares, B. G..; Briones, J. R. *Polym. Test.* **2007**, *26*, 95.
19. Mohanty, A.; Srivastava, V.K. *Mater. Des.* **2013**, *47*, 711.
20. Mohanty, A.; Srivastava, V. K. *Int. J. Sci. Eng. Res.* **2012**, *3*, 11.
21. Asi, O. *Compos. Struct.* **2010**, *92*, 354–363.
22. Chen, C.; Morgan, A. B. *Polymer* **2009**, *50*, 6265.
23. Zhou, Y.; Pervin, F.; Rangari, V. K.; Jeelani, S. *Mater. Sci. Eng.* **2006**, *426*, 221.
24. Jiang, Z.; Zhang, H.; Zhang, Z.; Murayama, H.; Okamoto, K. *Composites* **2008**, *39A*, 1762.
25. Schmidt, P. W.; Height, R. *Acta. Crystallogr.* **1960**, *13*, 480.
26. Schmidt, P. W. *J. Appl. Crystallogr.* **1991**, *24*, 414.
27. Martin, J. E.; Hurd, A. J. *J. Appl. Crystallogr.* **1987**, *20*, 61.
28. Shibayama, M.; Kurokawa, H.; Nomur, S.; Muthukumar, M.; Stein, R. S.; Roy, S. *Polymer* **1992**, *33*, 2883.
29. Hudson, S. D.; Hutter, J. L.; Nieh, M. P.; Pencer, J.; Million L. E.; Wan, W. *J. Chem. Phys.* **2009**, *130*, 034903.
30. Lee, K. Y.; Kim, K. Y.; Hwang, I. R.; Choi, Y. S.; Hong, C. H. *Polym. Test.* **2010** *29* 139–146.
31. Yarovsky, I.; Evans, E. *Poly.* **2002**, *43*, 963.
32. Sun, L.; Gibson, R. F.; Gordaninejad, F.; Suhr, *J. Comp. Sci. Technol.* **2009**, *69*, 2392.
33. Han, J. T.; Cho, K. *J. Mater. Sci.* **2006**, *41*, 4239.